High Energy Density Physics 9 (2013) 523–527

Contents lists available at SciVerse ScienceDirect

High Energy Density Physics

journal homepage: www.elsevier.com/locate/hedp

Testing the reliability of non-LTE spectroscopic models for complex ions

Stephanie Hansen [a,*], G.S.J. Armstrong [b], S. Bastiani-Ceccotti [c], C. Bowen [d], H.-K. Chung [e], J.P. Colgan [b], F. de Dortan [f,g], C.J. Fontes [b], F. Gilleron [d], J.-R. Marquès [c], R. Piron [d], O. Peyrusse [h], M. Poirier [i], Yu. Ralchenko [j], A. Sasaki [k], E. Stambulchik [l], F. Thais [i]

[a] Sandia National Laboratories, Albuquerque, NM 87123, USA
[b] Los Alamos National Laboratory, Los Alamos, NM 87545, USA
[c] LULI, Ecole Polytechnique, CNRS, CEA, UPMC, F-91128 Palaiseau Cedex, France
[d] CEA, DAM, DIF, F-91297 Arpajon, France
[e] International Atomic Energy Agency, Nuclear Data Section, A-1400 Vienna, Austria
[f] Laser Gen, Institute of Physics, Czech Academy of Sciences, Na Slovance 2, Prague 8, Czech Republic
[g] DENIM, UPM, Madrid, Spain
[h] Univ. Bordeaux, CEA, CNRS, CELIA, UMR 5107, F-33400 Talence, France
[i] CEA, IRAMIS, Service "Photons, Atomes et Molécecules", Centre d'Etudes de Saclay, F-91191 Gif-sur-Yvette Cedex, France
[j] National Institute of Standards and Technology Gaithersburg, MD 20899-8422, USA
[k] Japan Atomic Energy Agency, 8-1 Umemidai, Kizugawa-shi, Kyoto 619-0215, Japan
[l] Faculty of Physics, Weizmann Institute of Science, Rehovot 76100, Israel

ARTICLE INFO

Article history:
Received 2 May 2013
Accepted 2 May 2013
Available online 11 May 2013

Keywords:
X-ray spectroscopy
Atomic kinetics
Plasma diagnostics
L-shell

ABSTRACT

Collisional-radiative atomic models are widely used to help diagnose experimental plasma conditions through fitting and interpreting measured spectra. Here we present the results of a code comparison in which a variety of models determined plasma temperatures and densities by finding the best fit to an experimental L-shell Kr spectrum from a well characterized, but not benchmarked, laser plasma. While variations in diagnostic strategies and qualities of fit were significant, the results generally confirmed the typically quoted uncertainties for such diagnostics of ±20% in electron temperature and factors of about two in density. The comparison also highlighted some model features important for spectroscopic diagnostics: fine structure was required to match line positions and relative intensities within each charge state and for density diagnostics based on emission from metastable states; an extensive configuration set was required to fit the wings of satellite features and to reliably diagnose the temperature through the inferred charge state distribution; and the inclusion of self-consistent opacity effects was an important factor in the quality of the fit.

1. Introduction

Spatially and spectrally resolved X-ray self-emission from hot, dense plasmas contains a wealth of information about the emitting plasma conditions: emission features that can be assigned to particular charge states and electronic configurations are direct evidence that those charge states exist in the plasma; line ratios can reveal the temperature- and density-sensitive charge state distribution and details about the atomic kinetics in particular ions; and line widths are sensitive to plasma densities and fields. While spatially and temporally resolved X-ray emission data can provide direct measurements of the emitting plasma's dimensions and duration, spectrally resolved line emission requires the use of atomic kinetics, or collisional-radiative, models to infer bulk plasma properties such as temperature and density. Typically, these models use plasma properties (composition, temperature, density, extent, etc.) as input, predict the resultant emission or absorption spectra, and optimize the agreement between measured and modeled spectra to diagnose the plasma.

Non-Local Thermodynamic Equilibrium (NLTE) atomic kinetic models are complex, requiring a definition of the electronic energy level structure that can range in its level of detail from fine-structure states with magnetic sublevels to average-atom orbitals with fractional populations. The energy level structure can also

* Corresponding author.
E-mail address: sbhanse@sandia.gov (S. Hansen).

1574-1818/$ – see front matter © 2013 Published by Elsevier B.V.
http://dx.doi.org/10.1016/j.hedp.2013.05.002

range in completeness from a simple structure that includes only the states that significantly contribute to emission (generally single excitations from the valence shell of each ion) to an extensive, statistically complete structure that includes many states with high principal quantum number n, inner-shell excitations, and multiply excited states that may not contribute much to the emission but play an important role in establishing channels for population transfer between states. At high plasma densities, models may incorporate density effects such as continuum lowering and pressure ionization. Whatever their structure, the energy levels are coupled via spontaneous, collisional, and radiation-driven processes that form a rate matrix whose solution determines the charge state balance and absolute emission intensities. The accuracy and completeness of the rate structure, too, can vary between models. Finally, the populations and radiative decay rates are used along with line profile calculations that may incorporate natural, thermal, density, instrument and/or opacity broadening to construct modeled spectra for comparison with measured data.

The difficulty of constructing reliable NLTE atomic models for complex, many-electron ions was dramatically illustrated in the results of the first NLTE code comparison workshop [1], which indicated a discrepancy of about 20 charge states among a collection of independent models for gold at electron density $N_e = 10^{21}$ cm^{-3} and electron temperatures T_e around 2 keV. In a series of follow-on workshops [2–7], this disagreement has been reduced to five or six charge states among all models and one or two charge states among the most sophisticated codes. These workshops have demonstrated the critical importance of complete dielectronic recombination channels for reliable kinetics modeling. And although diagnostically-relevant K-, L-, and M-shell spectra have been computed and compared at the workshops, the 2011 NLTE-7 code comparison workshop [7] was the first time that modelers were requested to diagnose the plasma conditions of a particular experiment based on a measured emission spectrum.

This work describes the results of the diagnostic comparison. It aims to assess the general reliability of plasma diagnostics based on atomic kinetic models by comparing the temperatures and densities diagnosed by a variety of models for a single measured L-shell emission spectrum from a well characterized, but not benchmarked, laser-produced Kr plasma. Details of the experiment [8] and description of various modeling strategies are given in Sec. 1. Brief descriptions of the models are given in Sec. 2, along with diagnosed plasma parameters and comparisons of calculated emission spectra with measured data. The concluding section offers a general discussion of modeling strategies and describes the essential features of reliable NLTE models for spectroscopic diagnostics.

2. Section 1: description of experiment and modeling strategies

A brief summary of the single laser-plasma experiment, diagnostics, and the measured data that were used for the diagnostic code comparison case are given here. More details and additional data from a variety of experiments are available in Ref. [8]. Fig. 1 illustrates the experimental setup: the plasma was created by focusing a flat-top, 1.5 ns duration, 0.53 μm, 230 J laser beam with an elliptical focal spot size of 1 mm (horizontal) by 150 μm (vertical) at the LULI2000 facility onto a Kr gas jet 750 μm from the exit plane of a 1 mm diameter supersonic gas nozzle. The laser intensity on target from the present experiment was 1.2×10^{14} W/cm^2 and the backing pressure of the nozzle was 4 bar, which produced a uniform ion density of about 5×10^{18} cm^{-3} at the laser focus site over a diameter of about 1 mm with the fairly uniform super-Gaussian profile schematically illustrated in Fig. 1. This density profile was

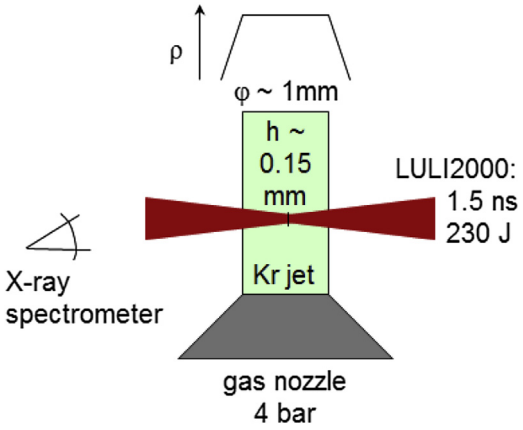

Fig. 1. Experimental schematic. LULI2000 was elliptically focused to 1 mm (horizontal diameter) by 150 μm (vertical height h) to create a steady-state Kr plasma 750 μm from the exit of a supersonic gas nozzle. The uniform ion density profile is notionally illustrated by ρ above. L-shell Kr spectra with spatial resolution along the laser axis were collected with an absolutely calibrated, time-integrating spectrometer.

measured with a Mach–Zehnder interferometer (see Ref. [9] for details).

The absorbed laser energy was measured by a calorimeter to be about 30% for this case. Spatially resolved, time-integrated L-shell Kr spectra were collected using an absolutely calibrated ADP crystal spectrometer with spectral resolution $\lambda/\Delta\lambda \sim 500$ and spatial resolution of 330 μm along the laser axis. Previous work [10] demonstrated that the spectral shape and intensity of keV X-ray photons in similar experiments remain fairly constant over the duration of the laser pulse. Time-resolved streaks of XUV emission spectra from 20 to 200 Å were also measured. Thomson self-scattering of the incident laser beam at 130° from an observed volume of 50(height) × 200(width) × 300(depth) μm^3 was collected to provide an independent estimate of the plasma conditions. For the present experiment, the Thomson scattering (TS) diagnostic indicated values of $T_e \sim 170$ eV, $N_{\text{ion}} \sim 5.1 \times 10^{18}$ cm^{-3}, and an average ionization $Z^* \sim 23$.

Although the plasma may have had spatial gradients that complicate spectral analysis and the cross-comparison of optical TS and X-ray diagnostics (see below), the extensive diagnostics provided strong constraints on the dimensions and duration of the source, an independent measurement of its ion density, and an absolutely calibrated emission spectrum. This collection of data offers a good balance for the NLTE workshop test case since it constrains the models but does not risk biasing their diagnostic results with fully characterized plasma conditions. As a result, the workshop case designed to test the consistency of diagnosed plasma conditions based on a variety of codes also elicited a variety of diagnostic inversion strategies. The workshop participants for the present experimental case used one of three different strategies: Four of the nine codes provided values only for T_e, using either the measured ion density of 5×10^{18} cm^{-3} or $N_e = Z^* \times N_{\text{ion}} \sim 1.3 \times 10^{20}$ cm^{-3} as fixed input and determining T_e by fitting the observed charge state distribution of the experimental spectrum ($Z^* \sim 25$). Four others provided values for both T_e and N_e, with T_e determined from the charge state distribution and N_e determined by fitting the relative intensities of Ne-like lines [11,12]. The remaining code result was based on an untraditional approach using a massively multi-parameter genetic algorithm to fix the level energies and line intensities, producing effective temperatures [13] among and within the ions. Three of the eight codes that used the more traditional approaches assumed optically thin emission and five included opacity effects. The test case results and the differences among particular codes will be discussed in the next section.

3. Section 2: models, synthetic spectra, and diagnosed plasma conditions

As described in the Introduction, collisional-radiative atomic models are complex systems that can have various levels of detail, accuracy, and completeness in their energy level and rate structures. While the completeness of the energy level structure is critical for equation-of-state applications [6,14], in the context of spectroscopic analysis it is useful to categorize models according to the level of detail with which they treat the diagnostically important spectral lines and features.

The nine contributed codes for the present case can be divided rather neatly into three categories. First, there are three hydrogenic models which use *nl*-based superconfigurations for the level structure and approximate rates to compute the populations. All three of these codes then use *nlj*-based expansions of the $nl - nl'$ transition arrays to compute spectra [14–16]. These models tend to be statistically complete, with high maximum values of n and extensive multiply excited states and dielectronic recombination channels. However, they are not generally spectroscopically accurate: the positions and relative intensities of spectral lines and features can vary significantly from measured values.

At the other extreme there are three highly detailed models based on fine-structure levels $nl\ ^{2S+1}L_J$ for the energy levels with relatively accurate rates [17–19]. Two additional fine-structure models contributed to another experiment in this workshop case [20,21] and are not extensively discussed here. Of the five total fine-structure models, three used data from the atomic structure code FAC [22] and two used data from HULLAC [23]. Because of the enormous number of fine-structure states for complex ions, these models tend to be less complete than the hydrogenic models. However, they tend to give much better agreement with measured line positions and relative intensities. In particular, they can provide accurate populations and line intensities for the density-sensitive metastable states in Ne-like ions that accumulate population via radiative cascades at low densities where collisional destruction is negligible [11,12].

Finally, there are three hybrid-structure codes based on combinations of fine-structure levels and relativistic (*nlj*) or non-relativistic (*nl*) configurations and superconfigurations [24–26], based on atomic data from a variety of sources [22,25,27,28]. These models tend to have both high statistical completeness and spectroscopic accuracy in predicted line positions, while the accuracy of their predictions for density-sensitive line intensities depends on whether their rate matrix retains fine-structure separation for metastable states.

The best-fit spectra from each of the nine contributed codes are given in Fig. 2 along with the experimental spectrum from the laser plasma described above. The modeled spectra have been broadened by the instrumental width and arbitrarily intensity-normalized for an overall best fit to the data. The temperatures and electron densities used to obtain the best-fit spectrum are listed next to each code's identifier along with their diagnosed Z^*. For the codes that included opacity effects, the photopumping and line-of-sight (horizontal) plasma dimensions are also given. The mean chord in the experimental plasma, which is expected to be the appropriate length scale to use for photopumping [29], was $<x> = 0.23$ mm and the maximum dimension along the X-ray spectrometer line of sight x_{LOS} was 1 mm. Three of the five codes that included opacity effects used different values for $<x>$ and x_{LOS}. All of these codes used the escape factor approximation for photopumping and transported the emission along the line of sight dimension. Photopumping and transport along the nominal experimental length scales leads to a reduction of about 50% in the main $3d - 2p$ resonance lines relative to other lines and features in the spectrum.

The hydrogenic codes shown in Fig. 2(a) all have generally poor agreement with the highly resolved spectral features evident in the experimental data. Hydrogenic codes tend to underestimate the populations of metastable states, which are not separated from resonant states in the rate matrix. Thus, density diagnostics based on metastable line ratios are not available to these codes and they generally under-predict the relative intensities of the $3s - 2p$ lines even when opacity effects that preferentially reduce the $3d - 2p$ lines are included. Although densities might have been independently diagnosed using the absolute intensities of the measured data, all of the hydrogenic codes used the measured ion density to determine N_e and the observed ionization balance to determine T_e. It is interesting to note that although these models were statistically complete, which is an important element of reliable calculations of Z^*, the three hydrogenic models contributed the extrema of the diagnosed temperature range (470 and 800 eV). The spread in diagnosed T_e is due to differences in the energy level structure in the M-shell ions, with the outlying "hydrogenic 3" code assigning higher energies to the first autoionizing states in those ions. This leads to smaller excitation–autoionization rates at a given temperature so that higher temperatures are required to reach the observed Ne-like charge states.

Fig. 2(b) shows that the fine-structure codes produced spectra with generally good agreement in the positions and relative intensities of the major spectral features. The two models that used the more traditional approach to diagnostics (solving the rate matrix at given plasma conditions) obtained very similar electron temperatures (600 and 650 eV) even with densities that differed by a factor of four. The model that took an unorthodox approach to fitting the spectrum inferred an effective temperature $T_{\rm eff} = 140$ eV using Boltzmann statistics for the level populations ($X_i \sim g_i \exp[-E_i/T_{\rm eff}]$). We noted that this is very close to the 143 eV effective temperature for 7 Å transitions predicted by simple collisional-radiative balance in a two-level system at $T_e = 600$ eV and $N_e = 1.3 \times 10^{20}$ cm^{-3} [30]. The two fine-structure models that took a more traditional approach obtained good fits to the data for the density-sensitive $3p - 2p$ electric quadrupole line [12] near 6.1 Å. Significant unresolved satellite emission features from Mg- and Al-like Kr around 6.5 and 7.1 Å are absent from all of the fine-structure models due to their limited completeness in the ion and multiply excited state structure. Finally, we note that two of these models (1 and 2) were based on data from FAC [22] and one (3) was based on data from HULLAC [23]. From the present comparison and additional analysis not detailed in this paper, it appears that both FAC and HULLAC provide high-accuracy data, with the level of configuration interaction included in the atomic structure calculations having a larger effect than the choice of code. The Los Alamos suite of codes [27,31] was found to provide similarly high-accuracy fine-structure data.

Fig. 2(c) shows that the spectral fits from the hybrid-structure models were also reasonably good. The diagnosed temperatures from the hybrid codes had a smaller spread than those among the hydrogenic codes but a larger spread than those among fine-structure codes. All of the hybrid codes provided diagnosed electron densities based on best fits to Ne-like line ratios and these densities varied by up to a factor of ten, with the codes that excluded opacity effects obtaining smaller densities. All of these models had both sufficient completeness to fill in most of the satellite emission around 7.1 Å (like the hydrogenic codes) and sufficient accuracy to match the positions of the strong resonance lines (like the fine-structure codes), although only one of these codes matched both the structure of the satellite emission features and the metastable Ne-like lines with fidelity comparable to the fine-structure codes. This underscores the importance of retaining separation in fine-structure states in the rate matrix as well as in

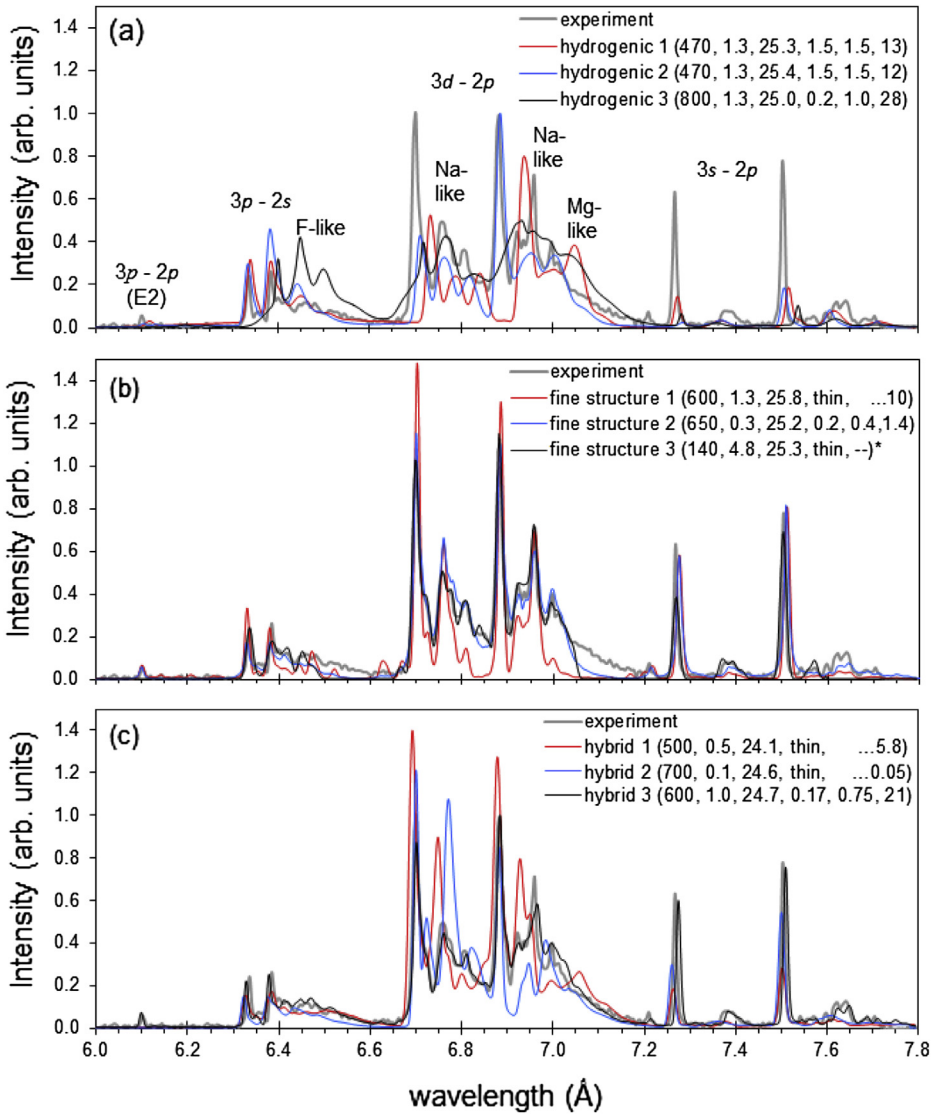

Fig. 2. Measured L-shell Kr emission spectrum (gray) and the best-fit emission spectra from nine independent NLTE atomic models. The plasma conditions associated with the fits are given after the code identifiers as T_e [eV], N_e [$\times 10^{20}$ cm^{-3}], Z^*, $<x>$ [mm], x_{LOS} [mm], and total radiative loss rates [TW/cm^2]. *The "fine structure 3" code used a unique approach to diagnose the temperature.

the emission spectrum, since averaging over the cascade and dielectronic recombination processes that populate these states destroys the non-statistical features of the populations.

The standard deviations of 20% in T_e and a factor of about two in density derived from the results of the eight codes that used one of the traditional diagnostic approaches are in line with typical accuracy estimates given for NLTE spectroscopic diagnostics. The diagnosed Z^* has a 3% standard deviation representing less than one charge state, which is better than typical agreement among codes at fixed plasma conditions. This suggests that ionization balances can be reliably determined by a variety of codes.

The radiative power loss of the experimental plasma was estimated to be about 20 TW/cm^3 based on the absolute intensity of the measured L-shell spectrum (which, according to the atomic kinetics models, contains about a third of the total emission) and assuming uniform emission over the duration of the laser pulse. As indicated in Fig. 2, the calculated total radiative power losses from all of the models that used $n_e \geq 10^{21}$ cm^{-3} varied from 10 to 30 TW/cm^3 and scaled approximately with n_e^2. Given the uncertainties in the absolute calibration and modeled spectral shape, the level of agreement between the experimental loss rate and those of models that used the measured ion density is quite good and supports the use of the measured density as a given parameter. This estimate for the experimental loss rates also provides a strong consistency check for the diagnosed plasma densities.

Although the measured ion density and radiative loss rates are consistent with the conditions diagnosed by most of the codes, we note that the electron temperature and Z^* measured by the Thomson scattering (TS) diagnostic are both significantly smaller than those diagnosed from the X-ray spectrum by the NLTE models. The TS Z^* of 23 is well outside the range supported by the X-ray emission, which suggests that the self-scattering is sampling a cooler portion of the plasma. In Ref. [8], it was proposed that hot spots formed by laser non-uniformities might account for both the X-ray emission and the Thomson scattering data. However, the NLTE model that is most consistent with the collection of experimental data (hybrid 3, which gave excellent agreement in both absolute and relative intensities with the measured spectrum using ion densities and plasma dimensions slightly smaller than measured and $T_e = 600$ eV) would not be able to simultaneously fit

all of the X-ray data using hot spots. If the hot spots were denser than the measured ion density to compensate for their smaller volume and recover the measured absolute intensities, the relative intensities of the metastable lines would decrease due to both smaller opacity effects and increasing collisional destruction of the metastable states. If, however, temperature gradients were present, both the X-ray spectrum and the XUV emission at 0.63 ns can be reasonably well matched by a uniform-density plasma that has a hot central core of 0.75 mm diameter and $T_e \sim 600$ eV surrounded by a cooler annulus of outer diameter 1.1 mm and $T_e \sim 60$ eV. The TS diagnostic might have sampled an intermediate region.

4. Conclusions

The complexity of NLTE atomic kinetics codes for many-electron ions has made reliable spectroscopic diagnostics for emission beyond the simpler K-shell ions – and reliable NLTE calculations for EOS and radiative transport used in plasma simulations – notoriously difficult. The code comparison presented here supports conservative accuracy estimates of $\pm 20\%$ in T_e and factors of about two in N_e for diagnostics based on fitting L-shell X-ray emission spectra. In support of the conservative nature of these estimates, we note that even smaller standard deviations of 10% in T_e, 50% in N_e, and 1% in Z^* were obtained for a second experimental case (4 bar, 360 J) that was modeled in the workshop but not detailed here.

In addition, this extensive comparison helps to establish the essential features of reliable collisional-radiative models and diagnostic approaches: Spectroscopic accuracy in line positions and NLTE relative intensities requires separation of fine-structure states in the calculation of both level populations and spectra. Including transitions beyond electric dipoles can provide additional density diagnostics and greater fidelity with data, and extensive configurations are required to capture unresolved satellite emission. Reliable calculations of the overall ionization balance require both statistical completeness and reasonable accuracy in the energy level structure. Opacity and gradient effects can significantly improve fits to spectral data, but their inclusion should be warranted by the entire collection of experimental data and additional experimental constraints should be introduced to prevent underdetermination of the inversion. In this spirit, measured spectra ought not to be modeled in isolation: the credibility of spectroscopic diagnostics can be enormously increased by consistency checks against all available experimental data including measured radiation powers, plasma dimensions, emission duration, and emission measured from diverse spectral ranges.

Acknowledgments

S.H. was supported by Sandia, a multiprogram laboratory operated by Sandia Corporation, a Lockheed Martin Company, for the United States Department of Energy's National Nuclear Security Administration under contract DE-AC04-94AL85000. The work of G.A., J.C., and C.F. was performed under the auspices of the United States Department of Energy under contract DE-AC52-06NA25396. Yu.R. was supported in part by the Office of Fusion Energy Sciences of the U.S. Department of Energy. A.S. was supported in part by JSPS (Japan Society for the Promotion of Science) grants No. 23340185 and 23246165. F.dD. was funded by Czech Republic's Ministry of Education, Youth and Sports to the ELI-Beamlines (ELI, CZ,1.05/1.1.00/02.0061) and EC OP CZ.1.07/2.3.00/20.0087.

References

[1] R.W. Lee, J.K. Nash, Y. Ralchenko, J. Quant. Spectrosc. Radiat. Transfer 58 (1997) 131.
[2] C. Bowen, A. Decoster, C.J. Fontes, K.B. Fournier, O. Peyrusse, Yu.V. Ralchenko, J. Quant. Spectrosc. Radiat. Transfer 81 (2003) 71.
[3] C. Bowen, R.W. Lee, Yu. Ralchenko, J. Quant. Spectrosc. Radiat. Transfer 99 (2006) 102.
[4] J.G. Rubiano, R. Florido, C. Bowen, R.W. Lee, Yu. Ralchenko, High Energy Density Phys. 3 (2007) 225.
[5] C.J. Fontes, J. Abdallah Jr., C. Bowen, R.W. Lee, Yu. Ralchenko, High Energy Density Phys. 5 (2009) 15.
[6] NLTE-6 Workshop, unpublished.
[7] H.-K. Chung, C. Bowen, C.J. Fontes, S.B. Hansen, Yu. Ralchenko, unpublished.
[8] S. Bastiani-Ceccotti, N. Kontogiannopoulos, J.-R. Marquès, S. Tzortzakis, L. Lecherbourg, F. Thais, I. Matsushima, O. Peyrusse, C. Chenais-Popovics, High Energy Density Phys. 3 (2007) 20.
[9] N. Kontogiannopoulos, École Polytechnique. Ph.D. Thesis (2007).
[10] C. Chenais-Popovics, V. Malka, J.-C. Gauthier, S. Gary, O. Peyrusse, M. Rabec-Le-Gloahec, I. Matsushima, C. Bauche-Arnoult, A. Bachelier, J. Bauche, Phys. Rev. E 65 (2002) 046418.
[11] U. Feldman, J.F. Seely, A.K. Bhatia, J. Appl. Phys. 58 (1985) 3954.
[12] B.K.F. Young, A.L. Osterheld, R.S. Walling, W.H. Golstein, T.W. Phillips, R.E. Stewart, G. Charatis, G.E. Busch, Phys. Rev. Lett. 62 (1989) 1266.
[13] M. Busquet, Phys. Fluids B 5 (1993) 4191.
[14] H.K. Chung, M.H. Chen, W.L. Morgan, Yu. Ralchenko, R.W. Lee, High Energy Density Phys. 1 (2005) 3.
[15] H.K. Chung, M.H. Chen, R.W. Lee, High Energy Density Phys. 3 (2007) 57.
[16] S.B. Hansen, J. Bauche, C. Bauche-Arnoult, High Energy Density Phys. 7 (2011) 27.
[17] E. Stambulchik, unpublished.
[18] Yu.V. Ralchenko, Y. Maron, J. Quant. Spectrosc. Radiat. Transfer 71 (2001) 609.
[19] A. Sasaki, Plasma Fusion Res. 8 (2013) 2401021.
[20] M. Poirier, F. de Dortan, J. Appl. Phys. 101 (2007) 063308.
[21] F. de Gaufridy de Dortan, Rapport CEA-R 6115, 2006, p. 3429.
[22] M.F. Gu, Astrophys. J. 590 (2003) 1131.
[23] A. Bar-Shalom, M. Klapisch, J. Oreg, J. Quant. Spectrosc. Radiat. Transfer 71 (2001) 169.
[24] S. Mazevet, J. Abdallah, J. Phys. B 39 (2006) 3419.
[25] O. Peyrusse, J. Phys. B 33 (2000) 4303. O. Peyrusse, J. Quant. Spectrosc. Radiat. Transfer 71 (2001) 571.
[26] S.B. Hansen, J. Bauche, C. Bauche-Arnoult, M.F. Gu, High Energy Density Phys. 3 (2007) 109. S.B. Hansen, Can. J. Phys 89 (2011) 633.
[27] J. Abdallah Jr., R.E.H. Clark, J.M. Peek, C.J. Fontes, J. Quant. Spectrosc. Radiat. Transfer 51 (1994) 1.
[28] H.A. Scott, S.B. Hansen, High Energy Density Phys. 6 (2010) 39.
[29] P. Hatfield, High Energy Density Phys. 6 (2010) 301.
[30] S.B. Hansen, K.B. Fournier, C. Bauche-Arnoult, J. Bauche, O. Peyrusse, J. Quant. Spectrosc. Radiat. Transfer 99 (2006) 272.
[31] D.H. Sampson, H.L. Zhang, C.J. Fontes, Phys. Rep. 477 (2009) 111.